Repair Techniques for Fusion Reactor Applications

Weldability tests were conducted on fusion reactor materials

BY M. H. TOSTEN, S. L. WEST, W. R. KANNE JR., AND B. J. CROSS

ABSTRACT. Fusion reactors, such as the planned International Thermonuclear Experimental Reactor, will require repair of irradiated components during their lifetime. Previous work has shown that welding on irradiated material causes cracking in the weld heat-affected zone due to the presence of helium. In the current study, measurements of the effects of helium (from tritium decay) on the weldability of Types 304 and 316LN stainless steel were made. Low-heat-input gas metal arc weld overlays and a series of autogenous gas tungsten arc stringer beads were made on 0.5-in.- (12.7-mm-) thick 304 and 316LN plates that were tritium-charged, aged, and outgassed in the same pressure vessel. The helium concentrations of both plates, as determined by helium mass spectroscopy, were approximately 90 appm. Measurements from weld cross sections revealed more extensive intergranular cracking in the heat-affected zones of welds on the 304 plate when compared to those on the 316LN plate. Weld porosity was also much greater in welds on the 304 plate. The large differences in the amount of helium embrittlement cracking associated with the two types of stainless steel may be related to differences in the high-temperature creep resistance of the alloys and/or the helium bubble microstructures present in the materials before welding. Weld porosity differences were also observed and can be rationalized by using weld convection arguments.

Introduction

Work at the Savannah River Site (SRS) has shown that the weldability of stainless steel using conventional welding processes is strongly affected by the presence of helium. This was evidenced initially in attempts to repair an irradiated reactor tank wall constructed of Type 304 stainless steel (Refs. 1, 2) — Fig. 1. Helium embrittlement cracking was observed in the weld heat-affected zones (HAZs) in the "repaired" areas. Subsequent research led to the development of a low-heat-input gas metal arc welding (GMAW) overlay technique suitable for welding on stainless steels, both irradiated and tritium charged and aged, with a minimum of underbead and toe cracking up to helium levels of 220 appm (Ref. 3). This technique employed an oscillating torch to produce a cladding of filler metal approximately 0.035 in. (0.9 mm) thick with a depth of penetration into the base metal of only 0.003 in. (0.08 mm).

Weldability with the overlay technique was compared at SRS with conventional gas tungsten arc welding (GTAW) and GMAW techniques. The welding methods were also compared for irradiated vs. tritium-charged-and-aged 304 stainless steel (Ref. 4). Results showed the overlay technique to be a significant improvement over conventional welding methods. Surface toe cracking was eliminated with the overlay technique. Furthermore, cracking, both toe and underbead, was much less in the tritium-charged-and-aged stainless steel than in the irradiated 304 stainless steel for a given helium concentration.

One material of choice for a next step fusion device is Type 316LN stainless steel. Limited data are available on the weldability of thick sections of this material in the presence of entrapped helium from either exposure to 1) neutron fluences and the generation of ^{4}He or 2) high-pressure tritium gas and the subsequent decay to ^{3}He. Investigations of the weldability of thin sections of 316 stainless steel doped with helium were carried out at the Oak Ridge National Laboratory (ORNL) in cooperation with Auburn University (Refs. 5, 6). These investigations showed that 316 stainless steel responds in a qualitatively similar way to 304L stainless steel when welded after helium impregnation. That is, both are embrittled by the helium and the embrittlement is intergranular due to the growth of helium bubbles on the grain boundaries. The weldability investigations at ORNL/Auburn were carried out on very thin (0.030-in.) material. Compressive stress applied during welding was shown to reduce or eliminate cracking in these thin sections. A threshold of 1 appm helium was suggested below which cracking would not occur for repair welds in irradiated 316 stainless steel.

The weldability of irradiated 304 and 316 stainless steels has also been investigated in other countries, particularly Japan. Results support the findings that heat input is important to reduce cracking (Ref. 7), that mechanical properties are affected by the helium embrittlement cracking (Ref. 8), and that the amount of cracking is proportional to the helium content. In another study (Ref. 9), a direct comparison of neutron-irradiated 304 and 316LN seemed to show that 304 was less susceptible to cracking in the weld HAZs when compared to 316LN at similar helium levels.

In the current comparison study, a series of 316LN and 304 stainless steel test plates were exposed to high-pressure tritium and aged to produce ^{3}He. Gas metal arc overlays were applied to the plates along with a series of GTAW stringer beads to accentuate embrittlement effects. This paper describes the results obtained from the analysis of helium embrittlement cracking observed at welds on 0.5-in. (12.7-mm) plates of both alloys.

KEYWORDS

Stainless Steel
GMAW
GTAW
Overlay Welds
Helium Embrittlement
Porosity

*M. H. TOSTEN (*michael.tosten@srnl.doe.gov) is *principal scientist, S. L. WEST is senior fellow engineer, and B. J. CROSS is manager, Nuclear Energy Programs, Savannah River National Laboratory, Washington Savannah River Co., Aiken, S.C. W. R. KANNE JR. recently retired from Savannah River National Laboratory.*

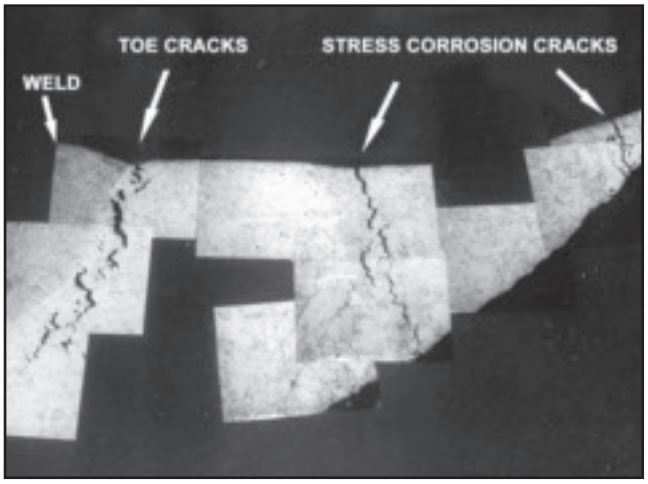

Fig.1 — Sample removed from a reactor tank wall at the SRS showing toe cracks and stress corrosion cracks near a gas tungsten arc weld.

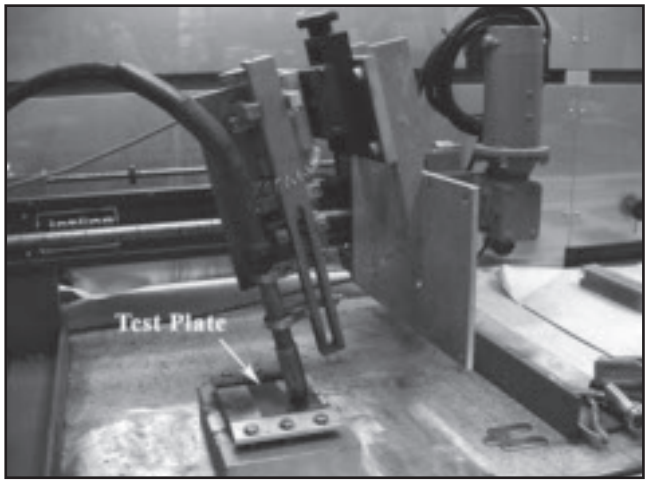

Fig. 2 — GMAW gun with oscillator. The test plate is located between the run-on and run-off tabs.

Table 1 —Alloy Composition (wt-%)

Type 304		Type 316LN-IG	
C	0.073	C	0.024
Mn	1.390	Mn	1.82
P	0.023	P	0.027
S	0.016	S	0.001
Si	0.520	Si	0.46
Ni	8.280	Ni	12.33
Cr	18.22	Cr	17.44
N	0.026	Mo	2.30
Fe	Bal.	N	0.06
		Ta	0.01
		Cu	0.20
		Co	0.17
		B	0.0008
		Fe	Bal.

Table 2 — Welding Conditions, 0.5-in. Plates

Alloy	Weld Type O/S*	Welding Wire	Oscillation Speed, S_0 (in./min)	Travel Speed, S_T (in./min)	I (amps)	E (volts)
304	O	308L	80	3.25	75	19
	S	None	N/A	25	100	18.3
	S	None	N/A	18	100	18.6
	S	None	N/A	6	101	18.4
	S	None	N/A	3.25	100	18.5
	S	None	N/A	18	31	20
316LN-A+	O	316L	80	3.25	69	19
316LN-B	O	316L	80	3.25	72	19
	S	None	N/A	25	100	19.4
	S	None	N/A	18	100	18
	S	None	N/A	6	100	17.8
	S	None	N/A	3.25	100	18.2
	S	None	N/A	18	32	21

* O — GMA overlay weld, S — GTA stringer bead
\+ A — Side of plate with stringer beads, B — underside of plate

Experimental Procedure

The welding substrate materials for this study were obtained from a special, high-carbon lot of Type 304 stainless steel used in a previous welding study (Ref. 3) and a special grade of 316LN (316LN-IG) proposed for use in the fabrication of ITER fusion reactor components. The starting materials were received as large plates in the solution annealed and quenched condition. The alloy chemistries are shown in Table 1. Pairs of identically sized plates of each alloy were electrical discharge machined from the as-received materials to serve as the helium-bearing substrate test matrix. These plates varied in thickness from 0.030 in. (0.8 mm) to 0.5 in. (12.7 mm) and measured 4.04 in. (103.4 mm) in length by 1.25 in. (31.8 mm) in width. The results presented in this paper are restricted to a pair of 0.5-in. (12.7-mm) plates. Run-on and run-off tabs to match each test plate were also machined from the as-received materials.

The two 0.5-in. (12.7-mm) plates analyzed in the current study were tritium charged and aged in the same vessel under identical conditions. The plates were held at 350°C for two weeks at a tritium overpressure of approximately 5000 lb/in.^{2} (34.5 MPa). At the completion of the charging run, the charging vessel was cooled to room temperature and depressurized. The plates were subsequently moved to a freezer for aging and stored at –23°C to minimize tritium off-gassing. Aging time for these plates was nine months. Following aging, both plates were vacuum outgassed for three weeks at 450°C to remove as much of the residual tritium as possible. Samples from 0.030-in.- (0.8-mm-) thick test coupons included in the charging run as well as samples from each 0.5-in. (12.7-mm) plate were analyzed for helium content using vaporization mass spectroscopy. An acid dissolution and beta scintillation technique was used to measure tritium levels in the test coupons after outgassing.

All welding was performed in a tritium fume hood using the experimental setup shown in Fig. 2. Two different type welds were used in this study — oscillated GMAW low-heat-input overlays and autogenous GTAW stringer beads. All welds were made using a shielding gas of 92% He, 7.5% Ar, 0.5% CO_2 at a flow rate 40 ft^3/h (18.9 L/min). Prior to welding, the plates were ground with 600-grit silicon carbide paper to provide a uniform surface finish and then clamped to a heat sink to provide adequate heat transfer and restraint. Overlay welds were made with 308L and 316L welding wire on the 304 and 316LN plates, respectively. Welding wires measured 0.035 in. (0.9 mm) in diameter.

GTAW stringer beads were made on the plates using a variety of conditions in an attempt to "bracket" any helium embrittlement effects. The conditions used for these welds, as well as those used for

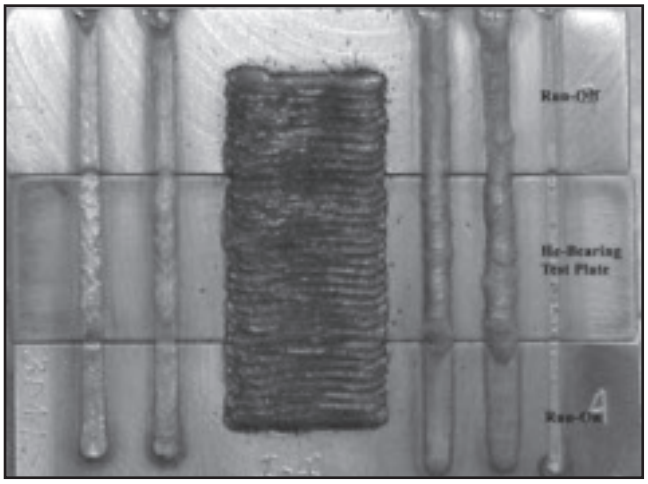

Fig. 3 — Typical weld/plate configuration. GMA overlay weld (center) with GTA stringer beads. The lower plate is the run-on tab (start of welds), the middle plate contains tritium/helium, and the upper plate is the run-off tab (end of welds).

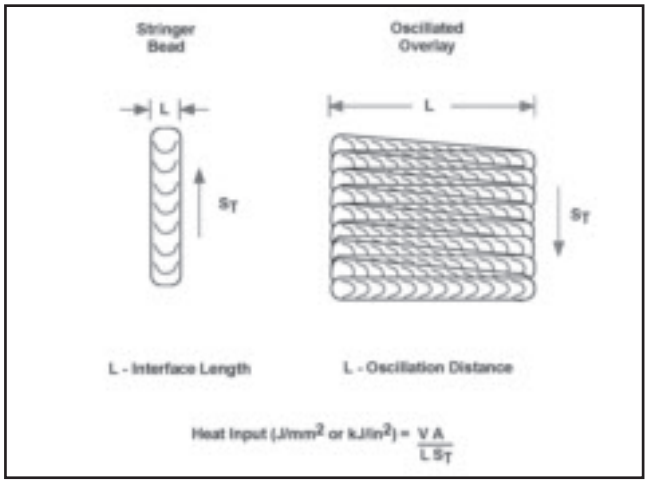

Fig. 4 — Schematic diagram illustrating the parameters used for heat input calculations for both GTA stringer beads and GMA overlays.

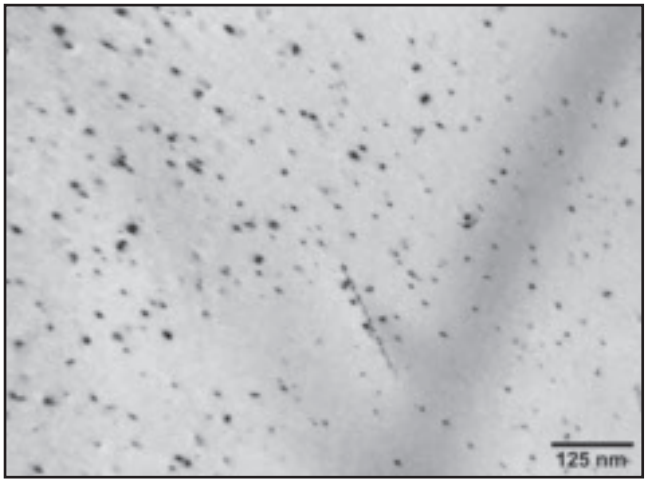

Fig. 5 — TEM image from a grain interior of the 304 material. The black dots are dislocation loops punched out by the formation of helium bubbles. Dislocation loops (or bubbles) were not observed in the 316LN.

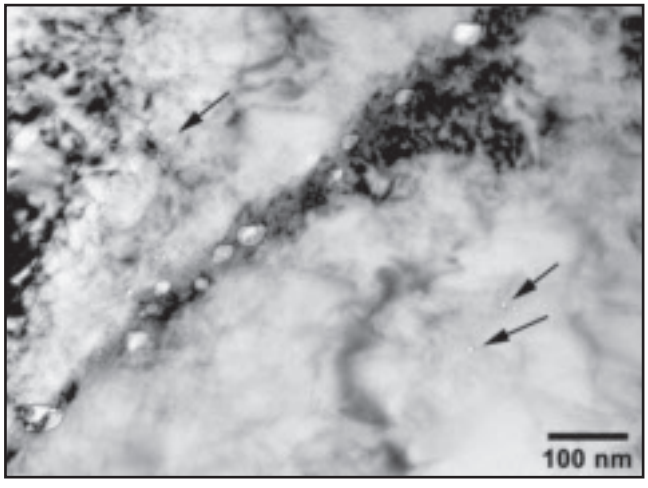

Fig. 6 — TEM image of large helium bubbles on a grain boundary and within the austenite matrix (e.g., at arrows) at about 0.010 in. (0.25 mm) below the GMA overlay interface on the 316LN plate.

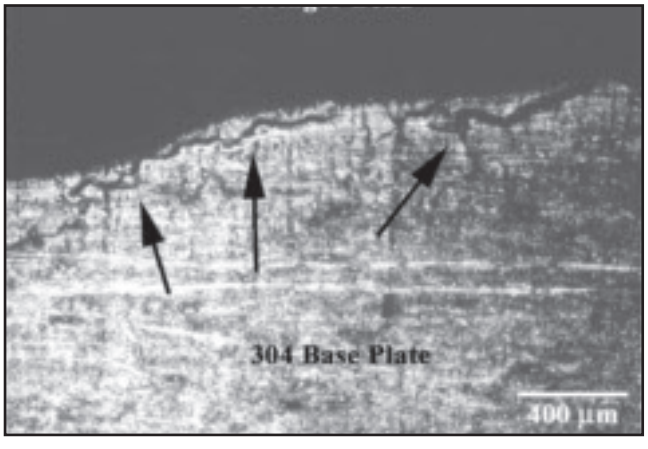

Fig. 7 — Toe cracking in the HAZ of the highest heat input stringer bead on the 304 base plate (Heat input: 136.6 kJ/in.^{2}).

the overlays, are listed in Table 2. Figure 3 is an image showing the series of welds made on the 0.5-in.- (12.7-mm-) thick 304 plate. The tritium/helium-containing plate is located between the two, uncharged run-on and run-off tabs. Similar plate and weld configurations were used for the 316LN welds except that a second overlay weld was applied to the underside of this plate. Weld heat inputs were calculated using the parameters illustrated in Fig. 4. This method allowed for a more direct comparison of the overlay welds to the stringer beads.

Welds were examined visually using a stereo microscope at 40X magnification to determine the extent of toe cracking in the HAZs. Additionally, metallographic cross sections were prepared from each weld using standard specimen preparation methods. All specimens were etched using a solution of 10% oxalic acid and water at 6 V DC to reveal microstructural features and helium embrittlement cracking. A montage of overlapping micrographs, taken at 50X magnification, was constructed for each weld cross section. Cracks and weld porosity were measured and counted using these micrographs.

Transmission electron microscopy (TEM) samples were prepared from be-

neath the GMAW overlays on both plates. Thin slices were cut from the weld HAZs in an orientation parallel to the weld interface. Slices were centered at approximately 0.010 in. (0.25 mm) and 0.050 in. (1.27 mm) from the interface. Control samples were sectioned in a similar manner, but from a region of each plate far removed from any welds. Disc specimens, measuring 3 mm in diameter, were punched from the slices and ground to a thickness of about 0.004 in. (0.1 mm). Specimens were polished to perforation with a twin jet electropolisher using a solution of 4 vol-% perchloric acid, 37 vol-% butylcellosolve, and 59 vol-% methanol. Polishing was accomplished using an applied potential of 35 V DC with the solution cooled to approximately –30°C. All specimens were examined in a JEOL 2010 operating at 200 kV.

Results

Helium and Tritium Analyses

The helium concentration in both steels was measured at various depths below the surface of the plates. The average helium concentrations, measured at approximately 0.005 in. (0.13 mm) below the surfaces, were 89.1 ± 6.8 appm and 87.6 ± 0.3 appm for the 304 and 316LN, respectively. Additional measurements from regions of each plate to depths of approximately 0.140 in. (3.6 mm) — approximate depth of the deepest weld root — yielded average helium concentrations of 89.7 ± 6.0 appm He for the 304 plate and 94.1 ± 3.0 appm for the 316LN plate. Residual tritium concentrations (after vacuum outgassing) measured from 0.030-in.- (0.8-mm-) thick test coupons were approximately 2.2 appm for the 316LN and 3.0 appm for the 304.

TEM Examination

Control samples from about 0.015 in. (0.4 mm) below the surface of the 316LN and 304 plates were examined using TEM. The microstructure of the 304 plate consisted of equiaxed grains containing a low number density of dislocations, dislocation loops, and stacking faults. Carbide precipitates were observed on some incoherent twin boundaries and high angle grain boundaries. Helium bubbles, measuring 1–2 nm in diameter were found in the matrix (homogeneously nucleated) and on dislocations in this material. Most of the matrix bubbles were associated with 10–20 diameter dislocation loops — Fig. 5. These defects were observed previously (Ref. 10) to form as a result of helium bubble nucleation and growth in the grain interiors. Helium bubbles were not observed on grain boundaries or at the carbide/matrix interfaces. The base microstructure of the 316LN plate resembled closely that of the 304 microstructure except that no carbide precipitates were observed. Helium bubbles were not identified in this material; however, a low number density of dislocation loops were observed in the grain interiors. Contrast differences resembling bubbles were noted at some dislocations but these were too indistinct to be identified as bubbles. As in the 304 plate, bubbles were not observed on the grai boundaries.

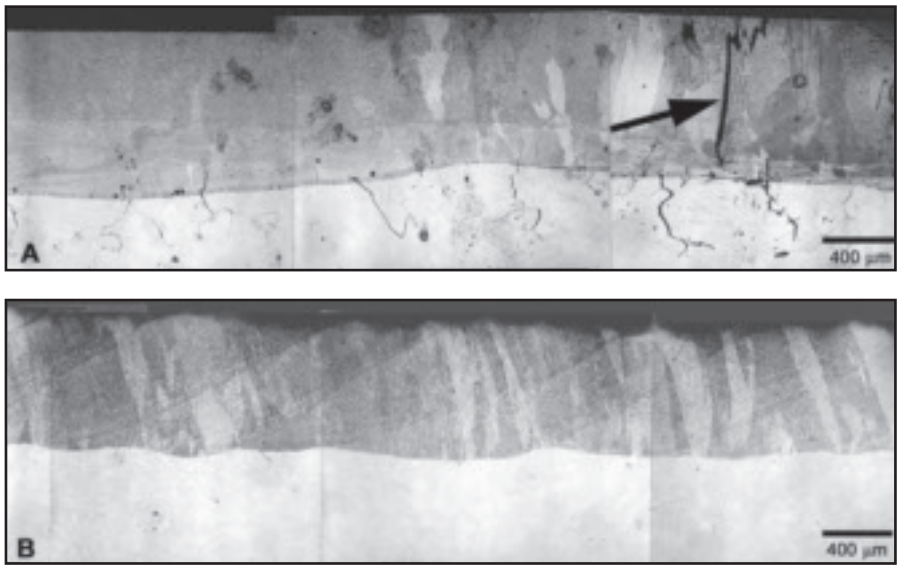

Fig. 8 — GMA overlay welds on helium-bearing plates: A — 304; B — 316LN. Much more cracking is observed in the 304 base metal. Some cracking in the weld metal can be seen at the arrow in Fig. 8A (Heat input: A — 23.4 kJ/in.², B — 21.5 kJ/in.²).

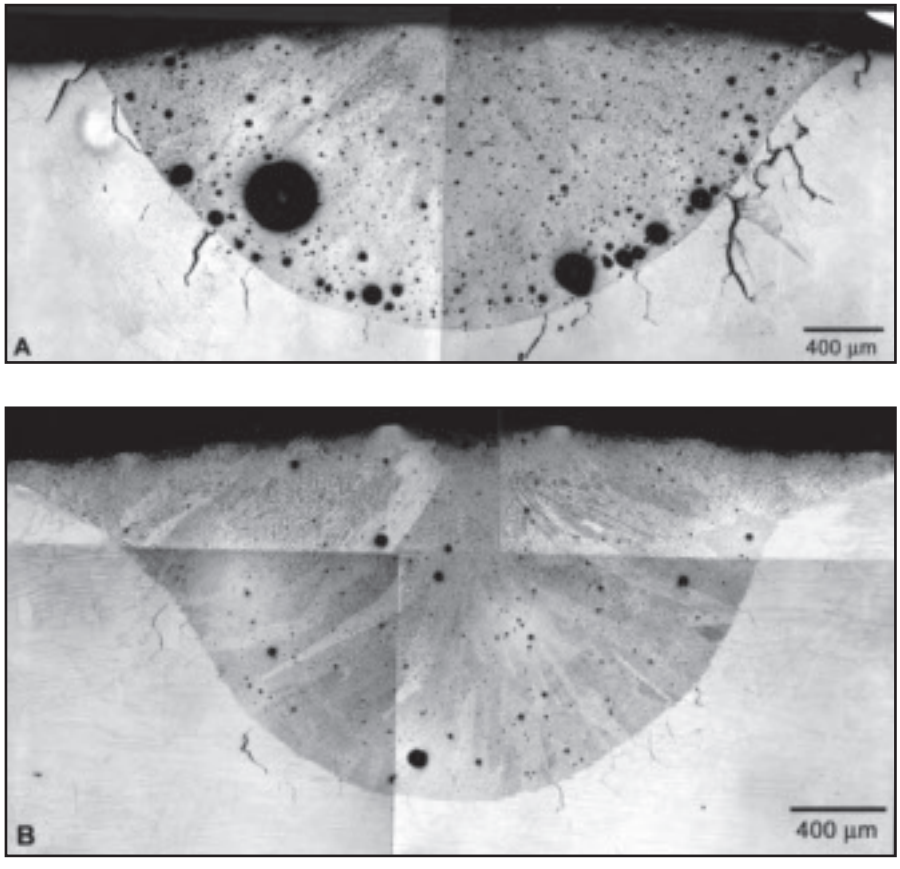

Fig. 9 — Cross sections of stringer beads: A — 304; B — 316LN. Note the differences in the number of underbead cracks, amount (and location) of porosity, and weld pool shape between the two welds. (Heat input: A — 28.7 kJ/in.², B — 28.2 kJ/in.²).

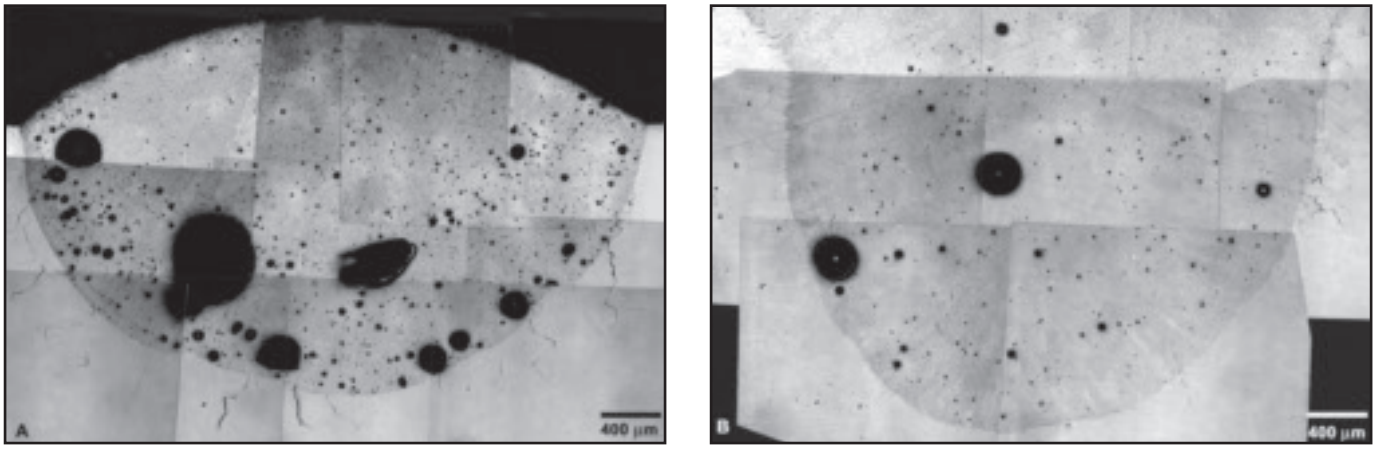

Fig. 10 — Cross-sections of stringer beads: A — 304; B — 316LN. These images further exemplify the differences in the GTA welds observed in the two steels. (Heat input: A — 84.5 kJ/in.², B — 91.3 kJ/in.²).

Examination of TEM specimens sectioned from approximately 0.050 in. (1.27 mm) beneath the weld overlay on the 316LN plate revealed an increase in dislocation density when compared to the control samples. An increase in dislocation density is caused by weld shrinkage stresses in the HAZ (Ref. 10). Additionally, small helium bubbles, 1–3 nm in diameter, were observed on some grain boundaries. Similar to the control sample, no obvious bubbles were observed in the grain interiors. Figure 6 is an image from 0.010 in. (0.25 mm) below the overlay. This image shows that large helium bubbles have formed on a grain boundary and within the matrix at this distance from the weld. Bubble growth occurred because of localized heating during welding and the diffusion of helium, tritium, and/or vacancies to preexisting grain boundary and matrix bubbles. Plastic deformation in the HAZ has also been shown to assist bubble growth via vacancy creation and dislocation/bubble interactions (Ref. 11).

Attempts to prepare thin foils from beneath the overlay weld on the 304 plate were unsuccessful. Severe cracking along grain boundaries and in regions of α' martensite, as determined by electron diffraction analysis, in the weld HAZ resulted in preferential thinning in these areas revealing little of the base microstructure or helium bubble distribution. Because of this a thorough microstructural comparison was not possible. However, the microstructure (dislocation substructure, helium bubble size, and distribution) that developed in the HAZ of the overlay weld on the 316LN plate was similar to that observed beneath overlay welds on 0.250-in. (6.35-mm) 304 plate material investigated in a prior study (Ref. 10).

Metallographic Examination

Analysis of the 0.5-in. (12.7-mm) plates at 40X magnification revealed no conclusive evidence of toe cracking in the HAZs of the GMAW overlays in either the 304 or 316LN material. However, extensive toe cracking was observed in the HAZs of the GTAW stringer beads. Figure 7 shows an example of toe cracking along a stringer bead in the 304 plate. These cracks were observed in the HAZ of the weld made using the highest heat parameters. Cracks, like those shown, were visible along the entire length of this weld in the helium-containing plate. In general, cracking was much more pronounced in the 304 plate than in the 316LN, with the amount of cracking in both plates increasing with weld heat input. Toe cracks were not observed in the HAZs of welds on the run-on or run-off tabs of either test plate.

Microscopic examination of the polished and etched weld cross-sections showed numerous intergranular cracks in the HAZ of the GMAW overlay on the 304 plate as seen Fig. 8A. Generally, cracks extended into the base metal by only a few grains. Infrequently, cracks also extended into the weld (e.g., Fig. 8A). This observation demonstrates that cracking took place after solidification of the weld pool and not during weld production. Some cracking was observed beneath the overlay on the 316LN plate but to a much lesser degree when compared to the 304 material — Fig. 8B. In contrast, cross sections made from the GTAW stringer beads revealed extensive intragranular cracking. Similar to the toe cracking, underbead cracking was much more pronounced in the HAZs of the GTA welds on the 304 plate when compared to the similar welds on the 316LN plate. These differences are illustrated in Figs. 9 and 10. Welds shown in each figure were made using identical weld parameters. As can be seen, much more cracking occurred in the HAZs of the 304 welds (compare Figs. 9A and 10A with Figs. 9B and 10B). Additionally, cracks extended into the 304 HAZ to a greater extent than in the 316LN, but crack lengths were still on the order of a few grains long. (It should be noted that underbead cracking did not occur on the run-on or run-off tabs.) Also evident from the welds in Figs. 9 and 10 are the differences in depth of penetration (or weld pool shape). The 304 welds tended to be shallower and had a wider weld root when compared to the welds on the 316LN plate. Furthermore, as expected, the weld pool size and depth of penetration increased with increasing heat input for all welds.

Another obvious difference in the welds was the amount, size, and location of porosity. The 304 welds contained considerably more porosity than the 316LN welds. Pores were generally much larger in the 304 welds and tended to be concentrated at the fusion boundary. Porosity in the 316LN appeared to be smaller and more uniformly dispersed throughout the weld pool. The large difference in porosity would suggest a difference in helium/tritium content existed between the test plates; however, helium levels were essentially the same (around 90 appm) for both materials. In addition, both test plates had been vacuum outgassed under identical conditions to remove most of the residual tritium available to contribute to bubble/pore formation.

Crack and Porosity Measurements

Crack analysis for both the overlays and the stringer beads was conducted by

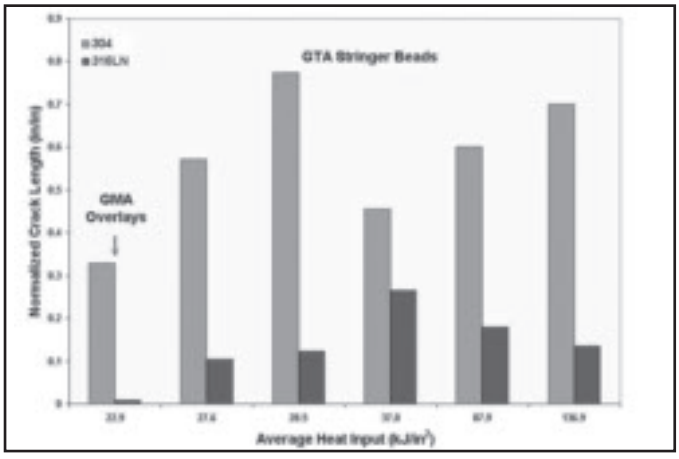

Fig. 11 — Comparison of the normalized crack length (in./in. of weld interface) for the GMA overlay welds and GTA stringer beads. Heat input values are the average of the actual heat inputs for 304 and 316LN welds at each targeted heat input level.

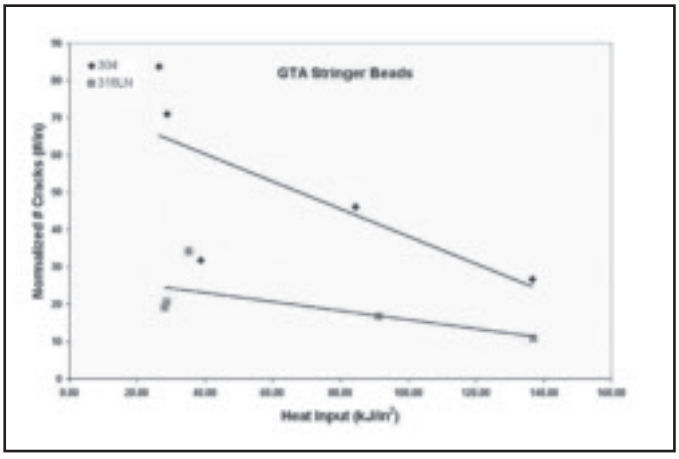

Fig. 12 — Total number of cracks per unit length of weld interface vs. heat input for the stringer beads on both plates.

measuring the total number and length of cracks visible in each metallographic cross section. To facilitate comparison, these measurements were normalized for differences in interface length (defined in Fig. 4). These data are summarized in Tables 3 and 4 and are shown graphically in Figs. 11–13. Data in each of these figures are also represented as a least squares fit forced to a straight line. Figure 11 shows the comparison of the normalized crack length, i.e., total measured crack length per unit length of interface for each heat input (denoted as the average heat input for each weld condition) for the overlays and stringer beads. Data for the stringer beads are further illustrated in Figs. 12 and 13, which show the total number of cracks per unit length of interface and the total crack length per unit length of interface vs. heat input, respectively.

Measurements taken from beneath the GMAW overlays show that there was about 12 times more cracking associated with the overlay on the 304 plate than with the overlay on the 316LN plate (Table 3). From Fig. 11, it can be seen also that the normalized crack length was about 33 times greater for the 304 when compared to the 316LN. A similar trend also existed for the GTAW stringer beads. Crack totals for these welds were about two to four times greater in the HAZs on the 304 plate when compared to like welds (similar welding conditions) on the 316LN plate (Fig. 12). Also, Fig. 13 shows that the normalized crack lengths were three to six times greater for the welds on the 304 plate.

Porosity measurements for both the overlays and stringer beads were made from micrographs of the weld cross sections. Porosity in these welds was arbitrarily defined as any pore greater than 20 μm in diameter, since smaller pores were difficult to discriminate from other microstructural features in the images. Limited porosity was observed in the overlay welds. In general, the overlay on the 304 plate contained slightly more pores (or inclusions) than the weld on the 316LN plate; however, the distribution of pores in both welds varied according to location in the weld weave. Porosity was more prevalent in the weld "toes" (where the torch changed direction) than at the center of the welds. Figure 14 is a plot of weld porosity vs. weld heat input for the stringer beads. It is evident from this figure that the amount of "visible" porosity, at any given heat input, was greater in the welds on the 304 plate than in the welds on the 316LN plate.

Table 3 — Underbead Crack Analysis Summary, GMA Cladding Welds

Plate Type[a]	I (amps)	E (volts)	Travel Speed (in./min)	Heat Input[c] (kJ/in.2)	He Conc. (appm)	Number Cracks/ Weld Interface Length (#/in.)	Total Crack Length/ Weld Interface Length(in./in.)
304	72	19	3.25	23.4	89.1	23.8	0.33
316LN-A[b]	69	19	3.25	21.5	87.6	1.9	0.01
316LN-B[b]	72	19	3.25	22.4	87.6	0.0	0.0

(a) ½-in.-thick plate, constrained during welding.
(b) A and B signify top (same side as GTA welds) and bottom of plate, respectively.
(c) Note: $J/mm^2 = kJ/in.^2 * 1.55$.

Discussion

The results of this study as illustrated in Figs. 11–13 indicate that Type 316LN is less susceptible to helium embrittlement cracking than Type 304 at comparable helium levels. The reasons for this behavior are not completely understood but may be related to differences in 1) the high-temperature creep properties of the two alloys and/or 2) the initial (prior to welding) helium bubble microstructures existing in the steels. During exposures to temperatures ($T \geq 0.4\ T_m$) bubbles can grow in size — particularly in the presence of an applied stress — leading to premature intergranular failure. The loss in elevated temperature tensile and creep ductility properties and the tendency for weld HAZ cracking have been attributed to the growth and coalescence of microvoids nucleated at grain boundary helium bubbles. The conditions exiting in the HAZs (e.g., high temperature and stress), during and after welding, provide the necessary driving forces to promote bubble/microvoid growth, coalescence, and subsequent intergranular failure. It is generally agreed that intergranular cavity growth occurs by either 1) a stress-induced cavity growth process with grain boundary self-diffusion as the rate controlling step (Ref. 12), 2) creep of the matrix immediately surrounding the cavity (Ref. 13), or 3) a process that couples grain boundary self-diffusion to a steady-state creep process (Ref. 14). In the present study, if one assumes that cavity growth is controlled by 2

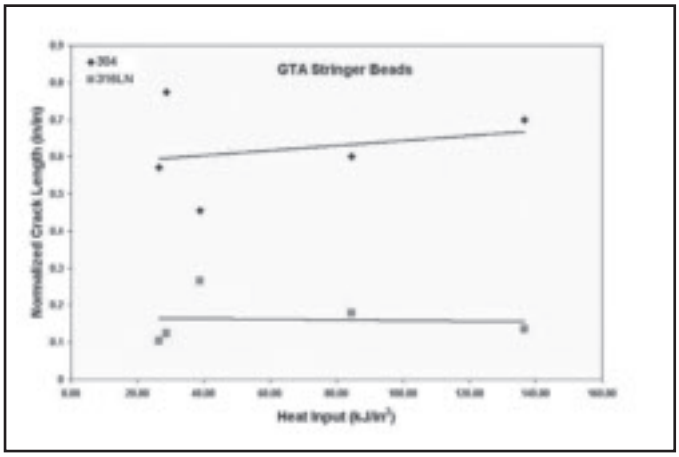

Fig. 13 — Normalized crack length vs. weld heat input for the stringer beads on both steels.

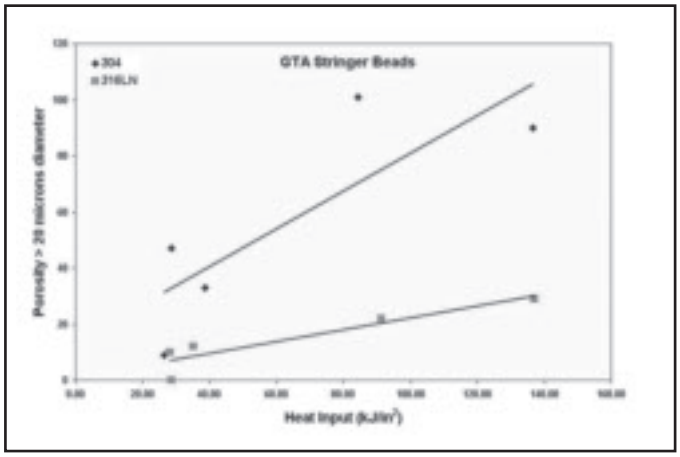

Fig. 14 — Porosity in stringer beads vs. weld heat input. More porosity in the 304 welds may indicate a higher helium content than in the 316LN plate.

Table 4 — Underbead Crack Analysis Summary, GTA Stringer Beads

Plate Type	I (amps)	E (volts)	Travel Speed (in./min)	Heat Input[a] (kJ/in.^{2})	He Conc. (appm)	Number Cracks/ Weld Interace Length (#/in.)	Total Crack Length/ Weld Interface Length (in./in.)
304	31	20	18	26.5	89.7	83.7	0.57
	100	18.3	25	28.7	89.7	70.9	0.77
	100	18.6	18	38.8	89.7	31.8	0.46
	101	18.4	6	84.5	89.7	46.2	0.60
	100	18.5	3.25	136.6	89.7	26.7	0.70
316LN	32	21	18	28.8	94.1	20.5	0.11
	100	19.4	25	28.2	94.1	19.0	0.12
	100	18	18	35.3	94.1	34.0	0.27
	100	17.8	6	91.3	94.1	16.7	0.18
	100	18.2	3.25	137.1	94.1	10.8	0.14

(a) Note: J/mm^2 = kJ/in.^{2} * 1.55

or 3 above, intergranular cracking in the HAZs of 316LN welds could be suppressed since 316LN is inherently more resistant to high-temperature creep than 304 because of the solid solution strengthening effect of ~ 2 wt-% Mo. Furthermore, although the starting microstructures of both alloys were very similar, carbides were observed only in the 304 material. A previous study (Ref. 10) of this material has shown that grain boundary carbides are potent nucleation sites for helium bubbles. It seems feasible that the presence of grain boundary carbides in the 304 plate could have led to an increase in the number of bubbles on the grain boundaries in that material. These bubbles would be available to act as additional microvoid nucleation sites, thus further reducing this alloy's resistance to helium embrittlement cracking.

Figure 14 (also see images in Figs. 9 and 10) shows that the 304 stringer beads contained significantly more porosity than the 316LN welds made using identical welding parameters. Porosity in welds on tritiated plates is associated with the trapping of helium (and tritium) in the solidified weld metal that was liberated during welding from the fusion and heat-affected zones. The results shown in Fig. 14 suggest that the helium concentration in the 304 plate was significantly greater than in the 316LN plate; however, multiple helium analyses on both plates indicates that this was not the case since both plates had a helium concentration of approximately 90 appm and nearly identical residual tritium levels (2–3 appm).

One possible explanation for the dramatic difference in the amount of trapped porosity in the two steels may be related to weld pool convective flow. Convection is influenced by four forces: 1) buoyancy force, 2) surface tension gradient force, 3) electromagnetic force, and 4) impinging force (Ref. 15). Variations in and combinations of these forces can have a great affect on the shape of the weld pool (depth of penetration) and the amount of retained porosity. Heiple and Burgardt (Ref. 16) have shown — for GTA welds using the same heat inputs and welding speeds — that weld penetration can be increased by modifying the surface tension temperature coefficient of the weld by adding surface-active agents. Additionally, Heiple and Roper (Ref. 17) observed shallower penetration in weld pools exhibiting a radially outward surface flow pattern, and deeper penetration in welds exhibiting a radially inward surface flow pattern. Through their modeling work, Kou and Wang (Ref. 18) have postulated that convective flow can reduce weld porosity. In welds where the convection pattern is radially outward (shallow penetration), bubbles can be caught in the solidification and become pores. Conversely, when the convective flow is radially inward (deeper penetration) bubbles can be swept out of the weld pool before being caught up in the solidification front.

Examination of welds in the current study seem to demonstrate, at least in principle, the two situations described by Heiple and Roper (Ref. 17) and Kou and Wang (Ref. 18). In all cases, the 304 welds exhibited less penetration and much more porosity when compared to the 316LN welds. Additionally, pores in the 304 weld were generally "trapped" near the bottom of the weld while pores in the 316LN weld were more uniformly dispersed in the weld pool. If one assumes that all "forces" affecting weld pool convention were essentially the same for both steels (i.e., identical weld parameters), these observations could indicate that weld pool convective flow was different for the two alloys — radially outward for the 304 (bubble trapping, shallow penetration) and radially inward for the 316LN (bubble removal, deeper penetration). However, based on the compositions

listed in Table 1, this explanation is counterintuitive since the higher S level in the 304 might be expected to produce deeper penetration welds (radially inward flow) and, hence, less bubble trapping when compared to the 316LN welds.

Porosity levels in the weld pools could also be related to the "availability" of helium to reach the weld pool. If more helium was present on the grain boundaries in the 304 stainless steel than in the 316LN as a result of, e.g., an increased number of carbides, then during the high-temperature excursion during the welding process more helium would be expected to move to the weld pool and eventually end up as additional porosity after solidification. Of course, if this were the case, then the number of nucleation sites for microvoids would decrease thus, inhibiting the embrittlement process to some degree.

Conclusions

A weldability comparison study of tritium-charged-and-aged Types 304 and 316LN stainless steels was conducted. The results of this research indicate that 316LN is less susceptible to helium-embrittlement cracking than the 304. This conclusion is supported by the following observations:

1. Extensive toe cracking was associated with the GTA welds with cracking more pronounced on the 304 plate. Toe cracking was not observed in the HAZs of the GMAW overlays on either the 304 or 316LN plate.

2. There were about 10 times more underbead cracks/in. in the HAZs of the overlay weld on the 304 plate compared to the 316LN plate with cracks generally limited to a few grains in length.

3. Underbead cracking was significantly greater in the HAZs of the GTAW stringer beads than the GMAW overlays on both plates. The total number of cracks was typically two to four times greater on the 304 plate when compared to the 316LN over the range of welding conditions. Similarly, normalized crack lengths were two to six times greater in the HAZs of 304 GTA welds.

The increased resistance to cracking of the 316LN can be rationalized in terms of its better resistance to high-temperature creep when compared to the 304. Differences in weld porosity and depth of penetration may be related to weld pool convection effects.

Recommendations

Further study is required to fully understand the fundamental reason(s) for increased porosity in the 304 GTAW stringer beads when compared to the 316LN welds at nearly the same helium levels. Additionally, the apparent differences in weldability of tritium-charged-and-aged 304 and 316LN stainless steel vs. irradiated 304 and 316LN (Ref. 9) needs to be investigated.

Acknowledgements

The authors would like to acknowledge Drs. M. J. Morgan, E. A. Clark, and M. R. Louthan, Jr., for their technical input during the course of this work; G. K. Chapman for the experimental setup and welding; and D. Z. Nelson and C. N. Foreman for the weld metallography.

This report is an account of work assigned to the U.S. Home Team under Task Agreement No. G 15 TT 96-05-15 FU within the Agreement among the European Atomic Energy Community, the Government of Japan, the Government of the Russian Federation, and the Government of the United States of America on Cooperation in the Engineering Design Activities for the International Thermonuclear Experimental Reactor ("ITER EDA Agreement") under the auspices of the International Atomic Energy Agency (IAEA). The report has not been reviewed by the ITER Publications Office.

The information contained in this article was developed during the course of work under Contract No. DE-AC09-96SR18500 with the U.S. Department of Energy.

References

1. Maloney, J. P. 1969. Repair of a nuclear reactor vessel. *Trans. Am. Nuclear Soc.* 12(supp.): 38-39.

2. Kanne, W. R., Jr. 1988. Remote reactor repair: GTA weld cracking caused by entrapped helium. *Welding Journal* 67(8): 33 to 39.

3. Franco-Ferreira, E. A., and Kanne, W. R., Jr. 1992. Remote reactor repair: Avoidance of helium-induced cracking using GMA welding. *Welding Journal* 71(2): 43 to 51.

4. Kanne, W. R., Jr., Chandler, G. T., Nelson, D. Z, and Franco-Ferreira, E. A. 1995. Welding irradiated stainless steel. *Journal of Nuclear Materials* 225(8): 69–75.

5. Wang, C. A., Grossbeck, M. L., Aglan, H., and Chin, B. A. 1996. The effect of an applied stress on the welding of irradiated steels. *Journal of Nuclear Materials* 239(12): 85–89.

6. Wang, C. A., Grossbeck, M. L., and Chin, B. A. 1995. Threshold helium concentration to initiate cracking during welding of irradiated stainless steel. *Journal of Nuclear Materials* 239(12): 59–68.

7. Asano, K., Nishimura, S., Saito, Y., Sakamoto, H., Yamada,Y., Kato, T., and Hasimoto, T. 1999. Weldability of neutron irradiated austenitic stainless steel. *Journal of Nuclear Materials* 264(1): 1–9.

8. Watanabe, K., Jitsukawa, S., Hamada, S., Kodaira, T., and Hishinuma, A. 1996. Weldability of neutron-irradiated Type 316 stainless steel. *Fusion Engineering and Design* 31(1): 9–15.

9. Morishima, Y., Koshiishi, M., Kashiwakura, K., Hashimoto, T., and Kawano, S. 2004. Re-weldability of neutron irradiated Type 304 and 316L stainless steels. *Journal of Nuclear Materials* 329-333: 663–667.

10. Tosten, M. H., and Kestin, P. A. 1992. Helium bubble distributions beneath GMA weld overlays in Type 304 stainless steel. *Proc. 24th Annual Technical Meeting of the IMS: Microstructural Science* 19. Eds. D. A. Wheeler, G. W. E. Johnson, D. V. Miley, and M. R. Louthan, Jr., pp. 3–12. ASM International, Materials Park, Ohio.

11. Goods, S. H., and Krafs, C. W. 1991. Helium-induced weld cracking in low heat input GMA weld overlays. *Welding Journal* 70(5): 123-s to 132-s.

12. Hull, D., and Rimmer, D. E. 1959. The growth of grain boundary voids under stress. *Philosophical Magazine* 4: 673–87.

13. Nix, W. D., Matlock, D. K., and Dimelfi, R. J. 1977. A model for creep fracture based on the plastic growth of cavities at the tips of grain boundary wedge cracks. *Acta Metallurgica* 25(5): 495–503.

14. Wang, J. S., Martinez, L., and Nix, W. D. 1983. The study on intergranular cavity growth controlled by the coupling of diffusion and power law creep. *Acta Metallurgica* 31(6): 873-81.

15. Messler, R. W., Jr. 1999. *Principles of Welding*. 291, New York, N.Y.: Wiley.

16. Heiple, C. R., and Burgardt, P. 1985. Effects of SO_2 shielding gas additions on GTA weld shape. *Welding Journal* 64(6): 189-s to 162-s.

17. Heiple, C. R., and Roper, J. R. 1982. Mechanism for minor element effect on GTA fusion zone geometry. *Welding Journal* 61(4): 97-s to 102-s.

18. Kou, S., and Wang, Y. H. 1986. Weld pool convection and its effects. *Welding Journal* 65(3): 63-s to 70-s.